(16) O'Reilly, J. M.; Teegarden, D. M.; Mosher, R. A. *Macromolecules* **1981**, *14*, 1693.
(17) Sundararajan, P. R. *Macromolecules* **1986**, *19*, 415.
(18) Vacatello, M.; Flory, P. J. *Macromolecules* **1986**, *19*, 405.
(19) Flory, P. J.; Sundararajan, P. R.; De Bolt, L. C. *J. Am. Chem. Soc.* **1974**, *96*, 5015.
(20) The experimental results of ref 8 are replotted here by taking the data in Figure 4 of ref 8 and converting these directly to the $F_x(q)$ plots in the usual manner[21] (taking the density ρ to be 1.22). Figure 9 of ref 8 underestimates the absolute values of $F_x(q)$ by ca. 10% in this regard.
(21) Yoon, D. Y.; Flory, P. J. *Polym. Bull.* **1981**, *4*, 693.
(22) Kirste, R. G. *Makromol. Chem.* **1967**, *101*, 91.
(23) Suter, U. W.; Saiz, E.; Flory, P. J. *Macromolecules* **1983**, *16*, 1317.

Uniaxiality Induced in a Strained Poly(dimethylsiloxane) Network

P. Sotta* and B. Deloche

Laboratoire de Physique des Solides, Université Paris-Sud, 91405 Orsay, France.
Received June 14, 1989; Revised Manuscript Received September 11, 1989

ABSTRACT: The orientational order generated in a uniaxially strained polymer network is described and discussed. Experiments have been performed on an end-linked poly(dimethylsiloxane) network, using the deuterium nuclear magnetic resonance technique (^{2}H NMR). We first recall that the resonance spectra observed in the absence of an external force reflect a local anisotropy of segmental motions, which may be related to the constraints associated with the presence of network junctions. When a uniaxial force is applied, a detailed analysis of the spectrum shows that the segmental motions become uniaxial around the external force direction. This experimental fact, which is inconsistent with noninteracting chain descriptions, is interpreted as new evidence for short-range orientational interactions between segments (introduced previously by Sotta et al. to account for free-chain orientation). A crude mean-field treatment including these interactions, together with the constraints associated to junctions, is proposed and compared with experiments.

1. Introduction

Much work, using several experimental techniques, has been devoted to investigating the anisotropy induced at a molecular scale by a macroscopic deformation in rubber polymer networks. Among these techniques, deuterium nuclear magnetic resonance (^{2}H NMR) in principle gives access to the anisotropy and time scales of individual molecular motions, by use of a probe nucleus (^{2}H) coupled solely with the orientation and motions of its host molecule. Thus ^{2}H NMR has been used to study the orientational order induced in rubber networks under a uniaxial stress. The main properties, which so far have been experimentally demonstrated in poly(dimethylsiloxane) (PDMS) networks, are now reviewed briefly.

Deuteriated probes, either conventional solvent molecules[1,2] or free PDMS chains,[3] have been dissolved in PDMS networks, wherein they undergo liquidlike translational diffusion (diffusion coefficient of the order 10^{-12} $m^2 s^{-1}$). A uniaxial orientational order is induced in these probe molecules upon elongation of the network; in other words, their orientational diffusion becomes, weakly but permanently, anisotropic and uniaxial around the applied force direction. This property, and specifically the free-chain orientation, has been interpreted as an experimental evidence for orientational interactions between chains, cross-linked or not, at a segment scale.

^{2}H NMR spectra obtained on network chains themselves exhibit more complex features, hitherto difficult to analyze quantitatively. Nevertheless, as the network is uniaxially stretched, these spectra likewise reveal a motional uniaxiality around the applied force direction.[4] Moreover, the orientation degrees measured on network chains and guest free chains (diffusing in the network) are the same under similar conditions.[3] This suggests that the correlations related to the orientational interactions quoted above may play a significant role in molecular dynamics, for both kinds of chains.

The purpose of this paper is to study in more detail the local uniaxiality reflected by the spectra of network chains, under uniaxial stress. Results particularly relevant in view of this scope are described in section 4, which emphasizes observations already published.[4] The observed stress-induced uniaxiality, as well as the free-chain orientation previously stated, is inconsistent with descriptions in terms of independent chains: this major discrepancy is illustrated in section 5. The observed induced uniaxiality is interpreted, as earlier, as a cooperative effect of the segmental short-range interactions already mentioned. These, modeled in a simple mean-field way, result in a uniaxial orientational field (of order $1/N$, where N is the average mesh size of the network). The motional anisotropy of a segment submitted to this field, additionally to constraints due to cross-link junctions, is computed; a qualitative description of ^{2}H NMR spectra is then proposed (section 6). However, the important discrepancies that remain between experimental results and modeling are discussed (section 7). These do not question the specificity of the ^{2}H NMR technique, which appears clearly when comparison is drawn with various optical techniques widely used in this area (section 7): these basically give access to ensemble averages of molecular orientation functions rather than to the distribution of these orientations, as is the case in ^{2}H NMR.

0024-9297/90/2223-1999$02.50/0

2. ^{2}H NMR Background and Local Orientational Order

The basic concepts of ^{2}H NMR in anisotropic fluids have been developed in numerous references.[5] Only elementary results relevant for our purpose are recalled herein. Due to its nonzero electric quadrupolar moment, the deuterium (^{2}H) nucleus possesses an electrostatic energy in the nonuniform electric field of the C–D bond. This nuclear interaction is a second-order tensor affixed to the molecule; it is expressed by the instantaneous Hamiltonian:[6]

$$H_Q = \nu_Q P_2(\theta)(3I_z^2 - 2) \quad (1)$$

I_z is the usual spin operator ($I^2 = 1$, so the effect of H_Q is to give a doublet of resonance lines). ν_Q, the static quadrupolar interaction constant, is of the order 200 kHz. θ is the instantaneous angle between the C–D bond and the steady magnetic field **B**, and $P_2(\theta)$ denotes the second Legendre polynomial:

$$P_2(\theta) = (3\cos^2\theta - 1)/2 \quad (2)$$

A *temporal* average over the molecular reorientations faster than $\nu_Q^{-1}(10^{-6}$–10^{-5} s) must be taken in eq 1, leading to an average interaction Δ given by

$$\Delta = \nu_Q\overline{P_2(\theta)} \quad (3)$$

Throughout the paper, overbars will denote temporal averages over fast motions. If the motions of the C–D bond are isotropic (isotropic liquid), Δ reduces to zero, and the transverse magnetic relaxation function (associated with fast fluctuations of the interaction) is an exponential with a relaxation time T_2 (corresponding, when Fourier transformed, to a Lorentzian line shape of line width T_2^{-1}). If the motions are anisotropic, the fluctuations no longer average the interaction to zero; this leads to a modulation of the transverse relaxation function, which may be expressed as

$$M_+(t) = M_0 e^{-t/T_2}\cos\Delta t \quad (4)$$

or as well, by Fourier transforming eq 4, to a doublet of Lorentzian lines, symmetric relative to the Larmor frequency, characterized by a splitting Δ.

In case of a nonuniform system, i.e., containing C–D bonds with distinct average axis and/or orientation degrees, there is one such doublet for each C–D bond (with a distinct orientation), and the resulting spectrum is the superposition of all these doublets. This *ensemble* average is denoted by angular brackets:

$$M_+(t) = M_0\langle e^{-t/T_2}\cos\Delta t\rangle \quad (5)$$

Note that the two steps described above must be clearly distinguished. First, the quadrupolar interaction for each nucleus is averaged by temporal fluctuations faster than 10^{-6}–10^{-5} s, leading to eq 4. Then, the relaxation function (eq 4) is integrated over all the nuclei present in the system, which leads to eq 5.

The second step vanishes out in a (uniform) *uniaxial* fluid system, wherein the motions of all C–D bonds consist in fast reorientations around the *same* symmetry axis;[7] in other words, all microscopic axes coincide with a macroscopic one, denoted by the unit vector **n**. In that case, the resulting spectrum is a unique doublet whose splitting Δ may be expressed as

$$\Delta = \nu_Q P_2(\Omega)\overline{P_2(\vartheta)} \quad (6)$$

where Ω is the angle between the symmetry axis **n** and the magnetic field, **B**, and ϑ is the angle between the C–D bond and **n**. The $P_2(\Omega)$ dependence may then be used as a crucial test for the uniaxial character of the molecular motions. $\overline{P_2(\vartheta)}$ is the mean degree of orientational order (i.e., the so-called order parameter S of the uniaxial fluid).

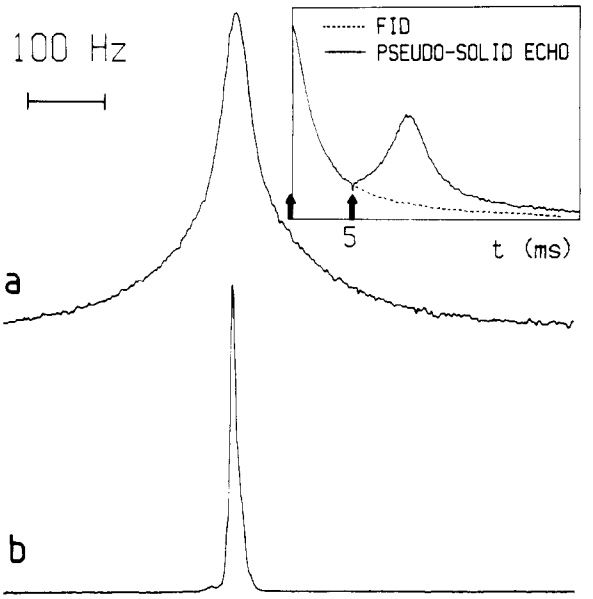

Figure 1. (a) ^{2}H NMR spectrum of perdeuteriated cross-linked chains in a dry PDMS network (average molecular weight between junctions: M_n = 10 500). The number of accumulations is 300, and the temperature, 298 K. The inset shows the pseudosolid echo obtained after a $(\pi/2]_x, \pi/2]_y)$ pulse sequence (arrows indicate pulse times). (b) ^{2}H NMR spectrum of perdeuteriated molten PDMS chains (M_n = 10 500).

3. Experimental Section

3.1. Samples. A dry poly(dimethylsiloxane) (PDMS) network was used, whose synthesis was outlined in detail in refs 8 and 9. It is an end-linked network, obtained by an hydrosililation reaction performed at a polymer volume fraction v_c = 0.71, that involves bifunctional PDMS precursor chains (average molecular weight M_n = 9700, molecular weight distribution M_w/M_n = 1.67) and bis(allyloxy)-3-[bis(allyloxy)methyl]-2,2-propylene oxide as a cross-linking agent. The network is therefore hexafunctional. About 26% of the chains are perdeuteriated. Note that the weight fraction of pendant chains was estimated to 15% from the fraction of the gel extracted after the cross-linking reaction.

3.2. NMR Experiments. They were performed on a Bruker CXP90 spectrometer, associated with a conventional electromagnet, at room temperature (T = 25 ± 1 °C). The Larmor frequency, ν_0, is 12 MHz, which corresponds to a magnetic field, **B**, of 1.8 T. Each spectrum is obtained by fast Fourier transforming the averaged free induction decay observed after a single $\pi/2$ pulse (whose length is about 8 μs), without any data manipulation. The line broadening associated with **B** inhomogeneity is less than 10 Hz and so is small with regard to the intrinsic half-height width of the spectrum (which amounts to about 70 Hz).

Sample elongation is performed as described earlier.[3] A uniaxial compression of the network has alternatively been achieved, which allows us to vary the angle Ω between the axis of the compression **F** and **B**.[4] Note that in practice the deformation remains low due to the fragility of the sample (deformation ratio $\lambda = L/L_0$ ranging from about 0.5 in compression to 2 in elongation).

4. Experimental Results

4.1. Relaxed Network. Figure 1a shows a spectrum obtained in the PDMS network in the absence of an exter-

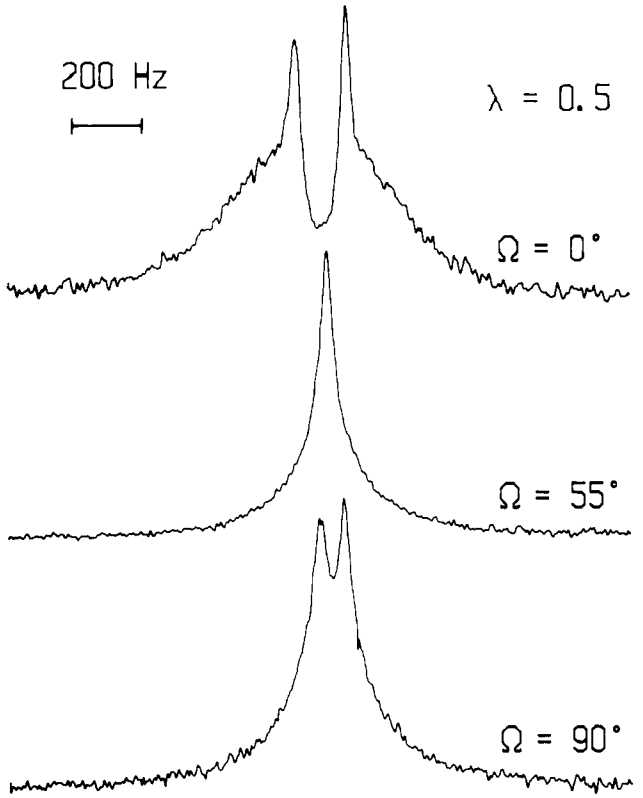

Figure 2. ^{2}H NMR spectra of a uniaxially compressed PDMS network (compression ratio $\lambda = 0.5$). The spectra correspond to three values of the angle Ω between the applied force, **F**, and the magnetic field, **B**: 0°, the magic angle 55°, and 90°.

nal constraint. The half-height line width is small (about 70 Hz) compared to the static interaction ν_Q (about 200 kHz), which means that a strong motional averaging is achieved.[10] However, the spectrum remains broad compared to the perfectly liquidlike resonance line (line width $\lesssim$ 10 Hz) obtained in a melt of the same PDMS chains (Figure 1b); moreover, the line shape in Figure 1a is not a Lorentzian one. Both features suggest that the spectrum may be associated with an incomplete averaging of the nuclear interactions. This point is corroborated by the response to an appropriate pulse sequence, which exhibits a well-shaped pseudosolid echo[11] (inset in Figure 1a). This pseudosolid echo reflects a modulation in the relaxation function, related to a nonzero residual nuclear interaction (see eq 4): it demonstrates that the molecular motions are slightly anisotropic on the ^{2}H NMR time scale (less than 10^{-6}–10^{-5} s), though the system is macroscopically isotropic.

4.2. Uniaxially Strained Network. Figure 2 displays ^{2}H NMR spectra obtained in the uniaxially deformed network (deformation ratio $\lambda = 0.5$), for different values of the angle Ω between the applied force, **F**, and the magnetic field, **B**. The most apparent pattern is that a well-resolved doublet structure ($\Delta \neq 0$) appears. It has already been pointed out that the doublet spacing, Δ, reproduces with great accuracy the $P_2(\Omega)$ dependence stressed in eq 6.[4] This demonstrates that the motions of the chain segments associated with the doublet are uniaxial around the applied force direction or, in other words, that the local symmetry axis **n** is along the force **F**. On the other hand, Δ varies linearly with λ^2–λ^{-1} without any threshold, i.e., as soon as the doublet becomes measurable.

However, together with this doublet, the spectra exhibit spectral wings, which become broader when the applied force is increased. Their presence is a general feature in all the networks studied (and is specific to the cross-linked chains). It remains to be specified to what extent the corresponding segmental motions are microscopically uniaxial around **F**.

Thus, a major result in this study is that the spectral wings themselves exhibit also clear indications of a $P_2(\Omega)$ variation: indeed, a dilatation of the frequency axis by a factor 2 in the spectra obtained with $\Omega = 90°$ allows us to superpose with good accuracy the wings obtained with $\Omega = 0°$, and a characteristic magic angle narrowing effect is also observed at $\Omega = 55°$ (Figure 2). This shows that the wings contain also contributions from motions which are uniaxial around **F** at a microscopic scale, though they correspond to different (higher) degrees of anisotropy, i.e., to various splittings: in other words, the wings reflect variations in the magnitude of the degree of order rather than in the local symmetry axis. However, the spectrum obtained at the magic angle ($\Omega = 55°$) is not a single Lorentzian (completely averaged) line and is identical with the one obtained in the relaxed state, within experimental uncertainties. Specifically, pseudosolid echos are obtained in that case as well as in the relaxed state, which means that some quadrupolar interactions are not averaged to zero at the magic angle. Some contributions to segmental motions, therefore, are not uniaxial around the applied force, **F**.

5. A Single-Chain Description

The aim of this section is to derive the ^{2}H NMR line shape, which would arise from a "kinetic" description of the chains, both in a relaxed and uniaxially constrained network. According to such a description, the chains interact only via their junctions, including both chemical and eventually physical ones, i.e., trapped entanglements. The junctions are allowed to fluctuate rapidly around their mean spatial positions, which are fixed. Then all the configurations compatible with this condition are supposed to be accessible and equally probable.[12] Indeed, the crucial point in this description is that certain constraint points along the chains are on average fixed in space at the NMR time scale, delimiting end-fixed chains (or subchains).[13]

The first step of the computation consists of estimating the anistropy along a network chain (or subchain) and the residual interaction associated with it. Then the contributions of all the chains are added together, given a proper distribution of chain (or subchain) end-to-end vectors.[14] Attention is focused on qualitative features of the spectra, so that a rather crude modeling of chain and network statistics has been adopted.

5.1. Anisotropy along a Single Chain. Each chain (or subchain) is represented by N freely jointed segments of length a. It is assumed for simplicity that each chain segment may be identified with an axially symmetric rigid rod, bearing one C–D bond along its axis and denoted by a unit vector **i**. This cylindrical symmetry may result from fast intrasegmental motions (isomerizations), such as rotations around the segment connecting two adjacent oxygen atoms in the PDMS chain. A weak force μ, which imposes an average end-to-end vector, **R**, is applied at the ends of a network chain to represent the effect of cross-link junctions. The free energy per segment, associated with the orientational entropy of the chain, is (expressed in kT units):

$$F_R^0 = \int f_R(\omega) \ln f_R(\omega)\, d\omega \qquad (7)$$

$d\omega$, the angular integration element, is normalized so that

$$\int d\omega = 1 \qquad (8)$$

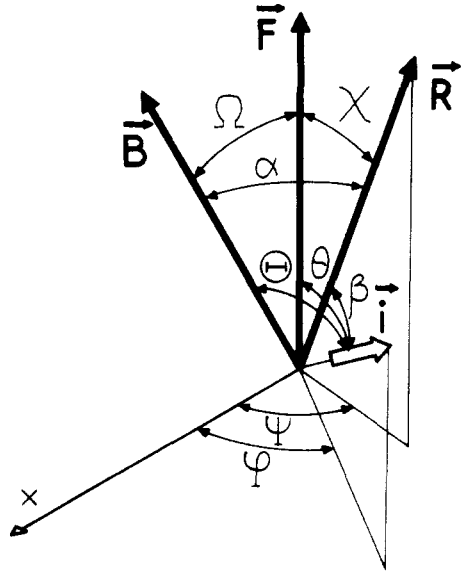

Figure 3. Different angular coordinates used to define the orientation of a segment **i** or of a chain end-to-end vector, **R**, with respect to the magnetic field **B**, or to the applied force, **F**.

$f_{\mathbf{R}}(\omega)$ is the orientational distribution function of the segment of a chain, whose average end-to-end vector is **R**: $f_{\mathbf{R}}(\omega)\,d\omega$ is the probability that a given segment lies in the direction $\omega(\beta,\gamma)$, within the solid angle $4\pi d\omega$. Note that $f_{\mathbf{R}}(\omega)$ only depends on the angle β between **R** and **i** (and not on the azimuthal angle γ), since the chain exhibits an average axial symmetry around **R** (see Figure 3). $f_{\mathbf{R}}(\omega)$ is normalized so that

$$\int f_{\mathbf{R}}(\omega)\,d\omega = 1 \tag{9}$$

$f_{\mathbf{R}}$ may be alternatively regarded as an instantaneous ensemble distribution over the whole chain or a temporal average over the successive orientations of one particular segment: chain motions are ergodic in this description, which implies that the segmental orientation is uniformly distributed along the chain. This property may be controversial in practice.[15] The constraint describing the cross-linked chain connectivity is

$$\int f_{\mathbf{R}} \cos\beta\,d\omega = \eta_{\mathbf{R}} = R/Na = r/N^{1/2} \tag{10}$$

where $\eta_{\mathbf{R}}$ is a reduced length of the chain and $r = R/R_0$ is the ratio of R to the root-mean-square end-to-end vector of the corresponding chain in the melt (ideal chain): $R_0 = N^{1/2}a$. The quantity to minimize in order to obtain the equilibrium distribution function $f_{\mathbf{R}}^0$ is thus

$$G_{\mathbf{R}}^0 = F_{\mathbf{R}}^0 - \mu_{\mathbf{R}} \int f_{\mathbf{R}} \cos\beta\,d\omega \tag{11}$$

The Lagrange multiplier, $\mu_{\mathbf{R}}$, may be identified with the weak force (in reduced units) introduced above. The functional minimization in eq 11 leads to

$$f_{\mathbf{R}}^0 = Z_{\mathbf{R}}^{-1} \exp[\mu_{\mathbf{R}} \cos\beta] \tag{12}$$

where $Z_{\mathbf{R}}$, the partition function, is (neglecting all terms of order higher than or equal to $\mu_{\mathbf{R}}^6$)

$$Z_{\mathbf{R}} = \int \exp[\mu_{\mathbf{R}} \cos\beta]\,d\omega = (\sinh\mu_{\mathbf{R}})/\mu_{\mathbf{R}} = 1 + \mu_{\mathbf{R}}^2/6 + \mu_{\mathbf{R}}^4/120 + O(\mu_{\mathbf{R}}^6) \tag{13}$$

The distribution function, $f_{\mathbf{R}}^0$, has thus been expressed in powers in $\mu_{\mathbf{R}}$. One may at this stage calculate the orientational second moment of the chain segments with respect to **R**:

$$\langle P_2(\beta)\rangle_{\mathbf{R}} = \int [(3\cos^2\beta - 1)/2] f_{\mathbf{R}}^0\,d\omega = \mu_{\mathbf{R}}^2/15 + O(\mu_{\mathbf{R}}^4) \tag{14}$$

This may alternatively be expanded in terms of the average reduced length of the chain, $\eta_{\mathbf{R}}$, which is given by

$$\eta_{\mathbf{R}} = (\delta \ln Z_{\mathbf{R}})/\delta\mu_{\mathbf{R}} = \mu_{\mathbf{R}}/3 - \mu_{\mathbf{R}}^3/45 + O(\mu_{\mathbf{R}}^5) \tag{15}$$

so that the following well-known expression is obtained:

$$\langle P_2(\beta)\rangle_{\mathbf{R}} = (3/5)\eta_{\mathbf{R}}^2 + O(\eta_{\mathbf{R}}^4) \tag{16}$$

5.2. Relaxation Function for a Single Chain. The relaxation function, $M_+(t)$, defined in eq 4 is computed in this section. The relaxation time, T_2, should a priori depend also on the end-to-end vector, **R**.[16] However, it may be assumed that the line shape is dominated by the distribution of the residual quadrupolar interactions rather than by the intrinsic width of each component: indeed, the largest T_2^{-1} value measured in the system (about 30 Hz) is small compared to the total width (a few 100 Hz) of the spectrum, i.e., to the modulations associated with residual interactions. So, in first approximation, the **R** dependence in T_2 may be neglected. What remains to compute is the interaction Δ given in eq 3, for the chain of end-to-end vector, **R**. Given the uniaxiality of the motions around **R**, the average quadrupolar order $\overline{P_2(\theta)}$ of the segments with respect to the magnetic field, **B**, may be expanded as

$$\overline{P_2(\theta)} = P_2(\alpha)\,\overline{P_2(\beta)} \tag{17}$$

where α is the angle of **R** with respect to **B** (Figure 3). Then, the temporal average $\overline{P_2(\beta)}$ in eq 17 is identified with the statistical average calculated in eq 16. This procedure may be achieved since the chain, considered as a statistical ensemble, is assumed to be ergodic, as quoted in section 5.1. This leads to the following expression for the residual interaction, $\Delta_{\mathbf{R}}$ (neglecting all terms of order higher than $1/N$):[17]

$$\Delta_{\mathbf{R}} = (3/5)\nu_{\mathbf{Q}}(r^2/N)\,P_2(\alpha) \tag{18}$$

The anisotropy at the segment scale, and thus the residual quadrupolar interaction (eq 3), has been averaged along the vector **R**, which represents the average direction of the chain: the interaction has been transferred from a local to a semilocal scale.[18]

5.3. Relaxation Function for the Network. The distribution of residual nuclear interactions is therefore related to that one of the end-to-end vectors **R**. According to eq 5, an integration must now be performed over the spatial (static) distribution of these vectors:

$$M_+(t) = M_0 \int h(\mathbf{R})\,d\mathbf{R}\,e^{-t/T_2} \cos\Delta_{\mathbf{R}}t \tag{19}$$

The spatial integration element, $d\mathbf{R}$, is $r^2\,dr\,d\omega$. In the absence of an external force, the normalized distribution of the vectors **R** is assumed to be isotropic Gaussian:

$$h(\mathbf{R}) = 4\sigma^3\pi^{1/2}e^{-\sigma^2r^2} \tag{20}$$

For Gaussian chains, σ^2 equals 3/2. When an external force **F** is applied, the end-to-end vectors are assumed to deform affinely, the volume element remaining constant; thus, for an elongation ratio λ, the distribution (eq 20) becomes

$$h_\lambda(\mathbf{R}) = 4\sigma^3\pi^{1/2} \exp[-(\sigma^2r^2/\lambda^2)[\lambda^3 - (\lambda^3 - 1)\cos^2\chi]] \tag{21}$$

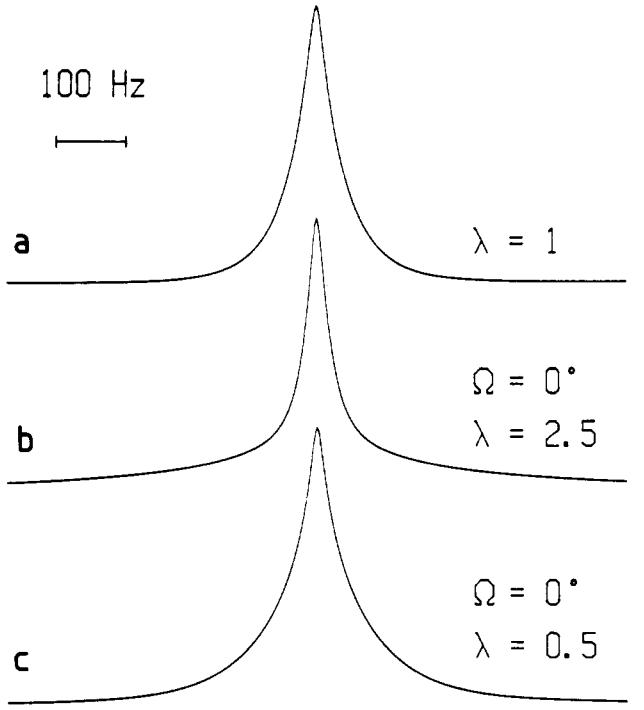

Figure 4. Spectra computed according to eq 22: (a) in the relaxed state ($\lambda = 1$); (b) in a uniaxially elongated state ($\lambda = 2.5$); (c) in a uniaxially compressed state ($\lambda = 0.5$), with **F** along **B** ($\Omega = 0°$). Affine deformation of the junctions has been assumed. Mean (reduced) average end-to-end distance: $\sigma^2 = 3/2$. Number of chain segments: $N = 20$. Relaxation time: $T_2 = 30$ ms.

where χ is the angle between **R** and **F**. The explicit formulation of the relaxation function is thus written as

$$M_+(t) = M_0 e^{-t/T_2} \int h_\lambda(\mathbf{R}) \cos [(3/5)\nu_Q(r^2/N)\, P_2(\alpha)\, t] \times r^2\, dr\, d\omega \quad (22)$$

Upon introduction of a (laboratory) fixed frame, with z axis along the external force **F** direction (Figure 3), the angles α and χ in eq 22 may be related to each other using the spherical harmonics addition rule:

$$P_2(\alpha) = \frac{4\pi}{5} \sum_{m=-2}^{2} (-1)^m Y_2^m(\Omega,0)\, Y_2^{-m}(\chi,\psi) \quad (23)$$

The Y_2^ms are the normalized spherical harmonics, $(\Omega,0)$ and (χ,ψ) denote, respectively, the orientations of **B** and **R** with respect to **F**, and the x axis of the laboratory frame has been set in the plane containing **B** and **F** (as indicated in Figure 3).

5.4. Comparison with Experimental Results. Since the line shape has been assumed to be dominated by the distribution of residual interactions, the parameter T_2 does not play a role in the computation of $M_+(t)$ (eq 22). So, the adjustable parameters in the description reduce to N, the number of segments per chain (or subchain), and σ^2, the average mean-square end-to-end distance of a network chain (or subchain). These parameters, which describe the network chain configurations, must be adjusted to values in accordance with the network molecular characteristics: then, σ^2 should be of the order 3/2 (ideal chains) and N of the order 50–100.

Relaxation functions in relaxed ($\lambda = 1$), elongated ($\lambda = 2.5$), and compressed ($\lambda = 0.5$) states have been computed from eq 22, using the values $\sigma^2 = 3/2$ and $N = 20$, and then Fourier transformed to give the spectra presented in Figure 4.

In the relaxed state ($\lambda = 1$), the calculated spectrum is not qualitatively different from the experimental one; specifically, a spectral broadening, related to the presence of residual interactions, is present. However, the line shape is not reproduced very accurately, and a rather low value of N (or σ^2) must be used in order that the half-height line width lie in the right range (about 70 Hz). This suggests that the Gaussian picture detailed above underestimates the residual interactions or, in other words, that the network chains are locally more oriented along **R** than Gaussian chains.

The line shape may be clarified in the following way. First, the integration over the direction of the end-to-end vectors **R** leads to a so-called Pake doublet with a splitting related to the modulus of **R** (i.e., a powder spectrum associated with an isotropic ensemble of equal interactions).[6] Then, the integration over the **R** moduli, given the distribution in eq 20 resumes in superposing powder spectra of various splittings. This results in the line shape represented in Figure 4a, similar to a so-called "super-Lorentzian" one.[19]

The calculated spectrum structure is not basically modified in the deformed network. Consider, for example, the case of **F** parallel to **B** (Figure 4b): the central part of the spectrum becomes narrower, whereas the wings become broader. This is a geometrical effect related to the anisotropy of the end-to-end vector distribution. Indeed, for each powder spectrum quoted above, the central part corresponds to vectors **R** at an angle 90° with respect to **B** (and then to **F**). The nuclear interactions are lowered in this direction. The wings correspond to vectors **R** along **F**: the interactions are magnified in this direction. However, the most noticeable feature is that *no doublet* structure appears, contrary to experimental evidence, whatever the angle Ω between the magnetic field, **B**, and the applied force, **F**.

The major point in this description is that the local anisotropy directions are distributed in the angular space: the motions of each segment are correlated with a particular chain direction. Then, the overall induced anisotropy comes from a anisotropic static distribution of the chain end-to-end vectors. As we have already pointed out, the uniaxiality reflected in the observed doublet structure is basically different: it actually means that each segment experiences the direction of the external force as a symmetry direction for its reorientations. So, the preceding analysis fails to account for the presence of a doublet. The minimum requirement in any attempt to model the segmental behavior is therefore to explain *at the same time* the line shape in the absence of constraint (at least qualitatively), the appearance of a doublet in the constrained state, and its $P_2(\Omega)$ dependence.

6. Orientational Interactions: A Mean-Field Description

Previous ^{2}H NMR experiments have shown that stress-induced orientation involves orientational interactions between chain segments, which are presumed to be short-range liquidlike interactions (van der Waals attractions, steric repulsions, ...). The effect of these interactions was described in terms of a weak self-consistent orientational field (with a nematiclike symmetry) coupled to the deformation.[1,2,20] This description is reformulated in this section, in order to take into account the complexity of segment motions, which results from the competing effects of an orientational field (related to short-range interchain interactions) and of constraints due to junctions.

6.1. Short-Range Orientational Interactions. The network free energy per segment is written (in kT units) in the mean-field form:

$$F = \int h(\mathbf{R})\, d\mathbf{R} \int f_{\mathbf{R}}(\omega) \ln f_{\mathbf{R}}(\omega)\, d\omega + \frac{1}{2}\int h(\mathbf{R})\, d\mathbf{R} \times \int h(\mathbf{R}')\, d\mathbf{R}' \int\int f_{\mathbf{R}}(\omega)\, f_{\mathbf{R}'}(\omega')\, V(\omega,\omega')\, d\omega\, d\omega' \quad (24)$$

The first term is the (kinetic) orientational entropy, already discussed above (section 5.1). The second term is the interaction energy, F_{int}, written in terms of one-segment distribution functions $f_{\mathbf{R}}(\omega)$ and $f_{\mathbf{R}'}(\omega)$.[21] $V(\omega,\omega')$ is an interaction potential between two segments i and j, which represents an average over all possible $\mathbf{r}_{ij}$, the spatial vector between i and j. Attention is focused herein on the part of the interaction potential that depends on the relative segment orientation. This anisotropic part is expanded in the spherical harmonic basis; given the assumed axial symmetry of each segment, it may be supposed that $V(\omega,\omega')$ depends only on the angle ϑ_{ij} between the segments i and j, and the first term may thus be written in the form[21]

$$V(\omega,\omega') = -UP_2(\vartheta_{ij}) \quad (25)$$

The parameter U characterizes the interaction strength ($U > 0$ if parallel packing is locally favored). It is then necessary to refer to the laboratory frame introduced in section 5.3 (Figure 3). A segment will be defined by its angle ϑ with **F** and an azimuthal angle, φ. When the spherical harmonics addition rule is used, the interaction energy, F_{int}, may be naturally rewritten in the form

$$F_{int} = -\frac{4\pi}{5}U\int h(\mathbf{R})\, d\mathbf{R} \sum_{m=-2}^{2} (-1)^m S_2^m \langle Y_2^{-m}\rangle_{\mathbf{R}} \quad (26)$$

The brackets with subscript **R** denote, as previously (section 5), a statistical average over a chain of end-to-end vector **R** (i.e., an average over the equilibrium orientational distribution, $f_{\mathbf{R}}^0$)

$$\langle Y_2^m\rangle_{\mathbf{R}} = \int d\omega\, f_{\mathbf{R}}^0(\omega)\, Y_2^m(\vartheta,\varphi) \quad (27)$$

and S_2^m is then an additional ensemble average over the **R** vectors

$$S_2^m = \int h(\mathbf{R})\, d\mathbf{R}\, \langle Y_2^m\rangle_{\mathbf{R}} \quad (28)$$

Note that the S_2^ms may be viewed as the five independent elements of a symmetric traceless tensor, which characterizes the mean degree of orientational order (the integrand in eq 26 has something to do with the second-order invariant of this tensor).[21] The mean-field expression eq 26 means that a segment is sensitive to an average orientational field. It is all the more justified as a given segment interacts with neighboring ones connected to many chains with different orientations.

6.2. Partition Function and Equilibrium Degree of Order. For a chain of end-to-end vector **R**, the partition function and then the equilibrium orientational coefficients $\langle Y_2^m\rangle_{\mathbf{R}}$ are determined by the same minimization procedure as in section 5.1, including now the interactions between chain segments. Following the lines developed in the Appendix, $\langle Y_2^m\rangle_{\mathbf{R}}$ is given by (in the order $\eta_{\mathbf{R}}^2$)

$$\langle Y_2^m\rangle_{\mathbf{R}} = \frac{(-1)^m}{5}[US_2^m + 3\eta_{\mathbf{R}}^2 Y_2^m(\chi,\psi)] \quad (29)$$

χ and ψ are the angles that define the orientation of **R** with respect to the laboratory frame introduced above (see Figure 3), i.e., with respect to **F**.

The average (macroscopic) values S_2^m of the orientational coefficients are obtained by integrating over the end-to-end vector distribution $h_\lambda(\mathbf{R})\, d\mathbf{R}$, which leads to a set of self-consistent equations. In a uniaxially strained state ($\lambda \neq 1$), the only nonzero value is S_2^0. The average degree of order is usually characterized by the quantity $S = \langle P_2(\theta)\rangle = (4\pi/5)^{1/2}S_2^0$, given by (in the order $1/N$)

$$S = [1/(5-U)](\sigma^{-2}/N)(\lambda^2 - \lambda^{-1}) \quad (30)$$

In other words, only S is coupled to the deformation of the network and is therefore expected to appear in the corresponding coupling terms in the free energy.[1,2]

6.3. ^{2}H NMR Relaxation Function. The average nuclear interaction, $\Delta_{\mathbf{R}}$, for a chain of end-to-end vector **R**, which involves the angle θ between the segment i and the magnetic field, **B**, is now computed. As has been done previously (section 5.2), intrachain statistical averages are identified with temporal averages. Then the spherical harmonics addition rule leads to

$$\overline{P_2(\theta)} = \frac{4\pi}{5}\sum_m (-1)^m\, Y_2^m(\Omega,0)\, \langle Y_2^{-m}\rangle_{\mathbf{R}} \quad (31)$$

where Ω denotes as previously the orientation of **B** with respect to **F**. When the $\langle Y_2^m\rangle_{\mathbf{R}}$s are replaced by their values given in eq 29, the following expansion is obtained (in the order $1/N$):

$$\Delta_{\mathbf{R}} = \nu_Q\left[\frac{3r^2}{5N}P_2(\alpha) + \frac{US}{5}P_2(\Omega)\right] \quad (32)$$

The first term in this equation is identical with the one calculated previously (eq 18). This part of the interaction, averaged along the end-to-end vector, **R**, according to the $P_2(\alpha)$ dependence, expresses the correlation between segmental motions and the vector **R**. It represents the effects of constraints due to cross-links. The second term in eq 32 represents the effect of the mean orientational field, characterized by the mean degree of order S given in eq 30. The corresponding part of the interaction is averaged along the direction **F** of the applied force, **F**, as reflected by the $P_2(\Omega)$ dependence. So, according to eq 32, two directions play a specific role in the segment motions.

6.4. Comparison with Experimental Spectra. The relaxation function for the network may be computed by the same explicit formula as eq 19, using the distribution function (eq 21) and the expression 32 for the residual interaction. Then a Fourier transform gives the resonance spectrum displayed in Figure 5b. The same parameters $N = 20$, $\sigma^2 = 3/2$, and $\lambda = 0.5$ as in section 5.4 have been used, together with a value of 160 Hz for the splitting, corresponding to an adjustable value $U/5$ of the order 10^{-1}. Qualitative features of the experimental spectra are well reproduced in this description. First, a doublet structure arises; it betrays the effect of the mean orientational field, US, which results from orientational correlations between segments. The doublet splitting, given by the second term in eq 32, reproduces the entire $P_2(\Omega)$ dependence. Moreover, according to eq 30, it varies as a $(\lambda^2 - \lambda^{-1})$ linear function.

Second, part of the interaction (corresponding to the first term in eq 32) is not averaged along **F** and so does not cancel at 55°. Note that the line shape obtained herein at 55° is the same as that one obtained previously in the absence of orientational interactions for the same λ (section 5.4). It is comparable to, though not strictly identical with, the one computed in the relaxed network.

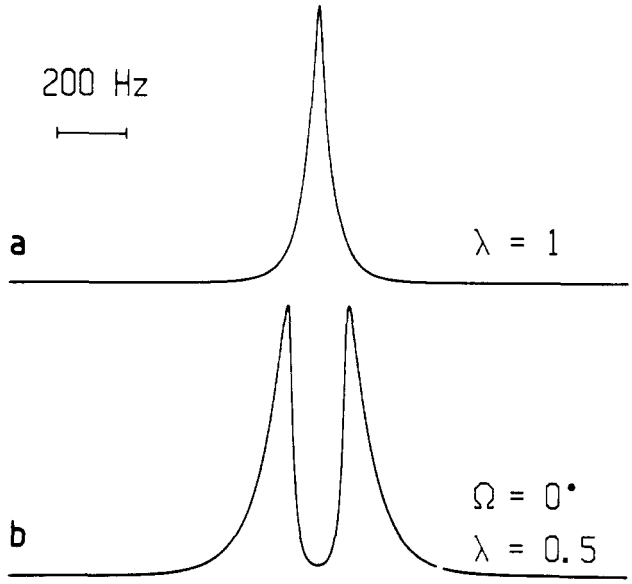

Figure 5. Spectra computed according to eq 22: (a) in the relaxed state; (b) in a uniaxially compressed state ($\lambda = 0.5$) in a direction $\Omega = 0°$ with **B**. The same conditions and parameters as in Figure 4 have been used. The effect of a uniaxial orientational interaction has been included in the residual interaction, according to eq 32, in the form of a doublet of splitting 160 Hz.

7. Discussion

7.1. Microscopic versus Macroscopic Uniaxial Order. A new property of rubber networks has been put into evidence, which leads to new insight in the segment orientation process. Indeed, in most descriptions of polymer networks, topological constraints at a semilocal scale (a few 10 Å) are attributed a predominent role in restricting the chain configurations. These constraints consist of cross-linking junctions with various geometrical restraints[22] or in confining potentials or tubes.[23-27] The external force is assumed to be transmitted at a molecular scale via these topological restrictions: the local constraints, and then anisotropy axis for segmental motions, are thus distributed in direction and magnitude, as sketched in Figure 6a. Consequently, the macroscopic uniaxiality induced upon stretching has its origin in the overall anisotropy of this distribution. Additional interactions at the segment scale (likely related to the details of the chain structure) are presumed to be negligible and are ignored.

It has been demonstrated (section 5) that the behavior observed at a segment scale is incompatible with the above picture. Indeed, the doublet structure and its $P_2(\Omega)$ dependence reflects uniaxiality at a local scale: on the NMR time scale (10^{-6}–10^{-5} s), **F** plays the role of a local symmetry axis for the reorientations of *each* segment. This characterizes a uniaxial fluid behavior, sketched in Figure 6b. To interpret this result, short-range orientational interactions between segments, belonging to different chains have been included, in addition to the distribution of constraints due to cross-link junctions. Upon elongation, these interactions generate a weak orientational field, which betrays the collective character of these interactions: the uniaxial symmetry is transferred at the segmental scale. Therefore, the segment motions are correlated with two competing directions, the one of the external force (via the orientational field) and the one of a topological constraint, related to cross-link junctions. According to eq 32, both contributions in the NMR spectrum are of the same order of magnitude $1/N$.

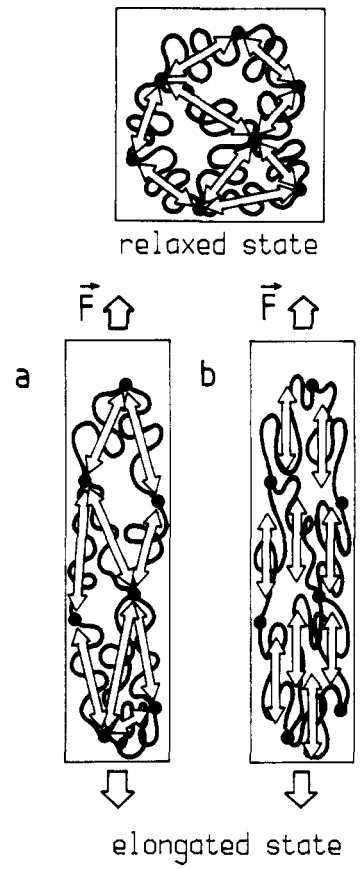

Figure 6. Two microscopic behaviors that may be distinguished with ^{2}H NMR: (a) According to a "kinetic" description, each chain retains a particular anisotropy direction in the deformed state, along its end-to-end vector. (b) In the uniaxial situation, which is observed experimentally, all the segments have the same symmetry axis for their reorientational motions.

7.2. Inhomogeneities in the System. As quoted in section 4.2, strong fluctuations in the magnitude of the degree of order are also reflected in the spectral wings. They are not accounted for by the above mean-field treatment, since no fluctuation in the orientational term has been included: clearly, the wings in the spectra are not reproduced very accurately. These fluctuations must be distinguished from the variations in the orientation directions related to junctions, i.e., due to the orientational distribution of end-to-end vectors. Several interpretations for such fluctuations may be suggested. Note, first, that the network chain polydispersity invoked in refs 5 and 15 is not expected to give a significant contribution to the wings, according to our interpretation. Indeed, recent ^{2}H NMR experiments in binodal PDMS networks show that the orientation degrees are the same on short and long chains.[28] It is more likely that, as pointed out in ref 15, the segmental orientation might be enhanced near the junctions, due to a stronger segment confinement in these areas. A specific role might also be attributed to dangling chains, whose ratio is not negligible in our system (about 15% in weight); they are doubtless oriented, as are free chains,[3] and may contribute to the doublet itself rather than to the wings. Last, inhomogeneities may result from the network structure itself:[29] some regions in the network might be more densely cross-linked than others, resulting in larger orientation. In order to be clarified, all these points need further experimental work, using, for example, networks selectively deuteriated near junctions or in the dangling chains.

7.3. Comparison with Optical Techniques. Various optical techniques have been used to study the segmental orientation in uniaxially deformed networks. In this section, the ^2H NMR approach will be compared to birefringence, infrared dichroism, and fluorescence polarization techniques. It is not intended here to compare quantitatively the results obtained in similar materials with these techniques but rather to discuss in a general way the nature of the quantities measured in each case. The specificity of ^2H NMR will therefore appear clearly.

The stress-induced birefringence (or optoelasticity) comes from an anisotropic (static or instantaneous) distribution of molecular polarizabilities, throughout the sample.[12] An *ensemble average*, i.e., the second moment of the chain segment orientational distribution, is obtained. Since the segmental polarizability is a second-order tensor, the optical anisotropy for one chain is equivalent to the intrachain-averaged quadrupolar interaction (section 5.2). However, in optoelasticity measurements, these intrachain quantities are then averaged over all the chains and their distribution cannot be analyzed:[30-32] the two averaging steps are not conceptually distinct, as in ^2H NMR. Consequently, the two pictures sketched in Figure 6 cannot be distinguished in these experiments, which might as well be interpreted in terms of a uniaxial orientational field (as shown in ref 1). Nevertheless, the question of short-range order has been discussed in the light of optoelasticity measurements.[33-35] The authors concluded that short-range effects, though eventually present, were too weak to be conveniently observed with this technique.

Infrared dichroism gives access to the orientational second moment of tensors affixed to the chain segment (corresponding to certain intramolecular vibrations).[36-37] This second moment is an ensemble-averaged quantity, and the same information on chain configurations as in birefringence is obtained. The specificity of this technique is to give specific pieces of information on local chain conformations (isomerizations), a point which was eluded in this paper.

Fluorescence polarization experiments make use of fluorescent probes attached to polymer chains and give access to correlation functions of the fluorescence moment orientation, especially[38-41]

$$G_{20}^{0} = \langle P_2(\alpha_0) \rangle$$

$$G_{22}^{0} = \langle P_2(\alpha_0)\, P_2(\alpha) \rangle \qquad (33)$$

G_{20}^{0} gives the second moment of the instantaneous orientational distribution of fluorescent moments. This quantity is basically analogous to that measured in birefringence experiments. G_{22}^{0} is a dynamic correlation function relating the orientation α_0 of a moment at a time t_0 and α at a time $t_0 + \tau$ (τ, the fluorescence lifetime, being of the order 10^{-9} s). So, the specificity of this technique, compared to the previous ones, is to give access to dynamic properties, as in NMR. However, the fluorescence intensity that is observed integrates contributions from all the chains, and the conditional probability distribution, $p_{av}(\omega/\omega_0)$, to move from orientation ω_0 (at $t = 0$) to ω (at $t = \tau$) is averaged over the whole system; the correlation function, G_{22}^{0}, may thus be written under the schematic form

$$G_{22}^{0} = \int\int P_2(\alpha_0)\, P_2(\alpha)\, p_{av}(\omega/\omega_0)\, d\omega_0\, d\omega \qquad (34)$$

On the contrary, ^2H NMR implies first an intrachain correlation function (defined over an intrachain conditional probability, $p_i(\omega/\omega_0)$, for each chain i), which is then integrated over all the chains, as detailed in section 2. These two steps, detailed in section 5, might be schematically expressed as

$$G_{22}^{0} = \sum_i \int\int P_2(\alpha_0)\, P_2(\alpha)\, p_i(\omega/\omega_0)\, d\omega_0\, d\omega \qquad (35)$$

So, the average processes involved in both techniques, NMR and fluorescence, are very different. It follows that the two situations sketched in Figure 6 cannot be distinguished by the fluorescence polarization either.

8. Concluding Remarks

The specific property of the uniaxially deformed polymer network, which has been put into evidence experimentally, is the uniaxiality of the segmental dynamics in the external force direction. This result is directly contained in the ^2H NMR line shape. It is by no means a model-dependent interpretation: indeed, the ^2H NMR line shape gives access to the distribution of local anisotropies, which contains more information than a mere orientational ensemble average and which is not accessible by other techniques cited above.

Then, this behavior has been interpreted as the cooperative effect of local orientational interactions, which induce a weak uniaxial orientational field in the deformed network. This orientational field contributes a $US^2/2$ term in the classical entropic free energy, i.e., a term of order N^{-2}, which appears as a perturbation of N^{-1} dominant terms. The main scope of the modeling was to clarify the picture of polymer networks, which is suggested by the experiments, and not to provide an accurate fit of experimental spectra. Specifically, the nature and values of the parameters, which should appear in a realistic network description, have not been discussed. As pointed out by Gottlieb and Gaylord,[42] these parameters are of two kinds: one related to the chain entropic elasticity and another one describing the additional chain confinement. As quoted in section 7.1, this later term is generally considered as acting at a semilocal scale (tube diameter of the order of the so-called distance between entanglements); what has been put into evidence herein is the effects of a local term, acting at the segmental level, which modify the *local* symmetry of segment motions.

Appendix

When interactions between chain segments are taken into account, the quantity to minimize with respect to the distribution $f_{\mathbf{R}}$, in order to get average quantities for a chain of end-to-end vector, $\mathbf{R}$, is, according to eqs 26 and 27

$$G_{\mathbf{R}} = F_{\mathbf{R}}^{0} - \int f_{\mathbf{R}}(\omega)\, d\omega[\mu_{\mathbf{R}} \cos\beta + (4\pi/5)U\sum_{m=-2}^{2}(-1)^m S_2^m\, Y_2^{-m}(\vartheta,\varphi)] \qquad (a.1)$$

where $F_{\mathbf{R}}^{0}$ is the orientational entropy of the chain in the absence of constraints (eq 7, section 5.1). The partition function for the chain may thus be written:

$$Z_{\mathbf{R}} = \int d\omega \exp[\mu_{\mathbf{R}} \cos\beta + (4\pi/5)U\sum_{m=-2}^{2}(-1)^m S_2^m\, Y_2^{-m}(\vartheta,\varphi)] \qquad (a.2)$$

The exponential is expanded in powers of $\mu_{\mathbf{R}}$ and US_2^m,

and the angular integrations lead to the following expression (in the order μ_R^4):

$$Z_R = 1 + \frac{\mu_R^2}{6} + \frac{\mu_R^4}{120} + \frac{4\pi}{25}U^2\sum_m S_2^m S_2^{-m} + \frac{4\pi}{75}\mu_R^2 U\sum_m S_2^m\, Y_2^{-m}(\chi,\psi) \quad \text{(a.3)}$$

The equilibrium values $\langle Y_2^m\rangle_R$ of the orientational coefficients, for a chain of end-to-end vector **R**, are obtained by relations of the form

$$\langle Y_2^m(\vartheta,\varphi)\rangle_R = (5/4\pi)(-1)^m\,(\delta \ln Z_R)/\delta(US_2^{-m}) \quad \text{(a.4)}$$

This leads to, in the order μ_R^2:

$$\langle Y_2^m\rangle_R = [(-1)^m/5][US_2^m + (\mu_R^2/3)\, Y_2^m(\chi,\psi)] \quad \text{(a.5)}$$

These may alternatively be expressed as functions of η_R, which is given by

$$\eta_R = \frac{\delta \ln Z_R}{\delta\mu_R} = \frac{\mu_R}{3} - \frac{\mu_R^3}{45} + \frac{8\pi}{75}\mu_R U\sum_m S_2^m\, Y_2^{-m}(\chi,\psi) + O(\mu_R^5) \quad \text{(a.6)}$$

The substitution of eq a.6 into eq a.5 leads to, in the order η_R^2

$$\langle Y_2^m\rangle_R = [(-1)^m/5][US_2^m + 3\eta_R^2\, Y_2^m(\chi,\psi)] \quad \text{(a.7)}$$

which is eq 29 in the text. The (macroscopic) average values S_2^m of these orientational coefficients are obtained by an integration over the end-to-end vector distribution, $h_\lambda(\mathbf{R})\,d\mathbf{R}$, following eq 28. Given the axial symmetry of the distribution $h_\lambda(\mathbf{R})\,d\mathbf{R}$, the only nonzero value is obtained for $m = 0$; the quantity $S = \langle P_2(\theta)\rangle = (4\pi/5)^{1/2}S_2^0$ is usually computed and is given by (in the order $1/N$):

$$S = \frac{1}{(5-U)}\frac{\sigma^{-2}}{N}(\lambda^2 - \lambda^{-1}) \quad \text{(a.8)}$$

Note that the quantities S_2^m ($m = 0$) may have been equated to zero a priori in eq a.1 and $\langle Y_2^m(\vartheta,\varphi)\rangle_R$ alternatively computed by

$$\langle Y_2^m(\vartheta,\varphi)\rangle_R = \int d\omega\, Y_2^m(\vartheta,\varphi)\exp[\mu_R\cos\beta + (4\pi/5)US_2^0\, Y_2^0(\vartheta,\varphi)] \quad \text{(a.9)}$$

The same results are of course obtained.

References and Notes

(1) Deloche, B.; Samulski, E. T. *Macromolecules* **1981**, *14*, 575.
(2) Sotta, P.; Deloche, B.; Herz, J. *Polymer* **1988**, *29*, 1171.
(3) Sotta, P.; Deloche, B.; Herz, J.; Lapp, A.; Durand, D.; Rabadeux, J. C. *Macromolecules* **1987**, *20*, 2769.
(4) Deloche, B.; Beltzung, M.; Herz, J. *J. Phys. Lett.* **1982**, *43*, L763.
(5) Samulski, E. T. *Polymer* **1985**, *26*, 177 and references cited therein. See also ref 16.
(6) Abragam, A. *The Principles of Nuclear Magnetism*; Clarendon Press: Oxford, 1961.
(7) A typical uniaxial fluid is an oriented nematic liquid crystal.
(8) Herz, J.; Belkebir, A.; Rempp, P. *Eur. Polym. J.* **1973**, *9*, 1165.
(9) Beltzung, M.; Picot, C.; Rempp, P.; Herz, J. *Macromolecules* **1982**, *15*, 1594.
(10) In solid polymer systems, line widths of about 100 kHz are indeed observed. See: Hentschel, R.; Sillescu, H.; Spiess, H. W. *Polymer* **1981**, *22*, 1516.
(11) Cohen-Addad, J. P.; Vogin, R. *Phys. Rev. Lett.* **1974**, *33*, 940.
(12) Treloar, L. R. G. *The Physics of Rubber Elasticity*; Clarendon Press: Oxford, 1975.
(13) Cohen-Addad, J. P.; Dupeyre, R. *Polymer* **1983**, *24*, 400.
(14) This description is formally identical with the analysis developed in: Lifchits, M. I. *Polymer* **1987**, *28*, 454.
(15) Some data suggest that the segments near junctions may be more oriented, though the uniaxiality has not been tested therein. See: Gronski, W.; Emeis, D.; Brüderlin, A.; Jacobi, M. M.; Stadler, R. *Br. Polym. J.* **1985**, *17*, 103.
(16) Cohen-Addad, J. P. *J. Chem. Phys.* **1974**, *60*, 2440.
(17) Intrasegmental isomerizations may result in additional motional averaging, i.e., an additional reduction of the residual interaction, Δ_R. Equation 18 holds in that case, replacing $3/5N$ by a numerical factor denoting the overall intrachain reduction of the interaction.
(18) Cohen-Addad, J. P.; Domard, M.; Lorentz, G.; Herz, J. *J. Phys.* **1984**, *45*, 575.
(19) Wenerström, H. *Chem. Phys. Lett.* **1973**, *18*, 41.
(20) Jarry, J. P.; Monnerie, L. *Macromolecules* **1979**, *12*, 316.
(21) de Gennes, P.-G. *The Physics of Liquid Crystals*; Clarendon Press: Oxford, 1974.
(22) Flory, P. J. *Polymer* **1979**, *20*, 1317 and references cited therein.
(23) Deam, R. T.; Edwards, S. F. *Philos. Trans. R. Soc. London, A* **1976**, *280*, 317.
(24) Edwards, S. F. *Br. Polym. J.* **1977**, *9*, 140.
(25) Marrucci, G. *Macromolecules* **1981**, *14*, 434.
(26) Gaylord, R. J.; Douglas, J. F. *Polym. Bull.* **1987**, *18*, 347.
(27) Graessley, W. W. *Adv. Polym. Sci.* **1982**, *46*, 67.
(28) Results to be published.
(29) Bastide, J.; Leibler, L. *Macromolecules* **1988**, *21*, 2647.
(30) Flory, P. J. *Statistical Mechanics of Chain Molecules*; Interscience: New York, 1969.
(31) Erman, B.; Flory, P. J. *Macromolecules* **1983**, *16*, 1601.
(32) Nagai, K.; Ishikawa, T. *J. Chem. Phys.* **1966**, *45*, 3128.
(33) Rehage, G.; Schäfer, E. E.; Schwarz, J. *Angew. Makromol. Chem.* **1971**, *16*, 231.
(34) Gent, A. N. *Macromolecules* **1969**, *2*, 263.
(35) Liberman, M. H.; Abe, Y.; Flory, P. J. *Macromolecules* **1972**, *5*, 551.
(36) Siesler, H. W. *Adv. Polym. Sci.* **1984**, *65*, 1.
(37) Jasse, B.; Koenig, J. L. *J. Polym. Sci., Polym. Phys. Ed.* **1979**, *17*, 799.
(38) Monnerie, L. In *Static and Dynamic Properties of the Polymeric Solid State*; Pethrick, R. A., Richards, R. W., Eds.; Reidel: Dordrecht, The Netherlands, 1982.
(39) Erman, B.; Monnerie, L. *Macromolecules* **1985**, *18*, 1985.
(40) Erman, B.; Monnerie, L. *Macromolecules* **1986**, *19*, 2745.
(41) Jarry, J. P.; Erman, B.; Monnerie, L. *Macromolecules* **1986**, *19*, 2750.
(42) Gottlieb, M.; Gaylord, R. J. *Polymer* **1983**, *24*, 1644.